# Effective design of managed realignment schemes can reduce coastal flood risks

*Joshua Kiesel*[a], Mark Schuerch[b], Elizabeth K. Christie[c], Iris Möller[d], Tom Spencer[c], Athanasios T. Vafeidis[a]*

[a] Department of Geography, Christian Albrechts Universität zu Kiel, 24118, Germany
[b] Lincoln Centre for Water and Planetary Health, School of Geography, University of Lincoln, Brayford Pool Campus, Lincoln, LN6 7TS
[c] Cambridge Coastal Research Unit, Department of Geography, University of Cambridge, CB2 3EN, UK
[d] Department of Geography, Trinity College Dublin, Museum Building, Dublin 2, Ireland
* Corresponding author

E-mail addresses:
kiesel@geographie.uni-kiel.de (J. Kiesel), mschuerch@lincoln.ac.uk (M. Schuerch), ekc28@cam.ac.uk (E. K. Christie), moelleri@tcd.ie (I. Möller), ts111@cam.ac.uk (T. Spencer), vafeidis@geographie.uni-kiel.de (A. Vafeidis)

Declarations of interest: none

**Abstract**

Managed realignment (MR) constitutes a form of nature-based adaptation to coastal hazards, including sea level rise and storm surges. The implementation of MR aims at the (re)creation of intertidal habitats, such as saltmarshes, for mitigating flood and erosion risks and for creating more natural shorelines. However, some evidence suggests that the desired coastal protection function of MR schemes (in terms of high water level (HWL) attenuation) may be limited and it was hypothesized that this was due to the configuration of the remaining seawalls, which we refer to as scheme design. The effects of scheme design on within-site HWL attenuation are

analysed for six scheme designs that differ in terms of breach characteristics and water storage capacity. The scenarios are established by manipulating the digital elevation model of the site topography to vary the configuration of the old defence line and the breaches.

Our results show that changes in scheme design, particularly storage area and number and width of breaches, had significant effects on the site´s HWL attenuation capacity. Decreasing the tidal prism by changing the number and size of breaches, with the site area kept constant, leads to increased modelled HWL attenuation rates. However, average HWL attenuation rates of > 10 cm $km^{-1}$ are only achieved when site size increases. The mean high water depth of each scenario, calculated by dividing tidal prism by MR area, explains most of the variation in average HWL attenuation between all scenarios. Attention to potential within-site hydrodynamics at the design stage will aid the construction of more effective MR schemes with respect to coastal protection in the future.

*Keywords: coastal wetland, high water level attenuation, coastal restoration, managed realignment, de-embankment, coastal protection*

## 1. Introduction

Managed realignment (MR) constitutes a form of nature-based adaptation for low lying coasts, aiming at the restoration or creation of intertidal habitats, such as saltmarshes, for the long-term management of flood and erosion risks. Saltmarshes can attenuate high water levels (HWL) (Smolders et al., 2015; Stark et al., 2016; Stark et al., 2015; Temmerman et al.,

2013), waves (Möller et al., 2014; Möller and Spencer, 2002; Rupprecht et al., 2017; Spencer et al., 2015) and provide flood water storage, thus contributing to mitigating coastal flooding. Furthermore, through the provision of intertidal habitats, saltmarshes provide additional services such as recreation, nutrient cycling, carbon storage, preservation of high water quality and biodiversity (Burden et al., 2013; Esteves, 2014; Luisetti et al., 2011; Spencer and Harvey, 2012).

Despite these multiple benefits, the assessment to what extent MR schemes provide their desired functions is difficult, as data on long-term individual project performance are scarce and of limited geographic coverage. In combination with societal and political resistance (Cooper and McKenna, 2008; Ledoux et al., 2005), the limited evaluation of MR may explain why the wider implementation is still hindered by funding constraints, availability of suitable land and uncertainties related to natural coastal evolution (Esteves and Williams, 2017). Nevertheless, MR schemes have been increasingly implemented in several countries, with large scale examples in Belgium (Sigma Plan, 2011), the USA (Day et al., 2007; EPA, 2013), Germany (Schernewski et al., 2018a; Schernewski et al., 2018b) and the UK (Cross, 2017; Esteves and Thomas, 2014; Turner et al., 2007). In December 2015, a total of 140 European sites were established (Esteves and Williams, 2017). In the UK, for example, the *Online Managed Realignment Guide* listed 51 MR projects in 2013 (Esteves and Thomas, 2014) which increased to 74 MR sites by 2019 (ABPmer, 2019). This growing interest needs to be accompanied by more comprehensive and longer-term monitoring, which could help to evaluate the sustainability and performance of MR and thus inform better MR design.

71 So far, there have been various types of MR scheme designs. These can be grouped into four
72 classes, namely: (1) the complete removal of flood defences; (2) single breach schemes; (3)
73 schemes with more than two breaches; and (4) regulated tidal exchange. The latter is
74 excluded from the analysis presented in this paper, as the primary aim of regulated tidal
75 exchange in Europe constitutes habitat creation (Esteves and Williams, 2017). The remaining
76 three approaches have been characterised by various objectives, such as the creation of more
77 natural shorelines, the promotion of biodiversity and, particularly in the UK, the
78 enhancement of flood protection (including the reduction of flood protection costs and flood
79 storage provision) (ABPmer, 2019; Esteves, 2013; Ledoux et al., 2005).
80 Across all different scheme designs, studies have shown that restored saltmarshes within MR
81 schemes are different from their natural counterparts. These studies have identified
82 differences in vegetation properties (Garbutt and Wolters, 2008; Mazik et al., 2010; Mossman
83 et al., 2012), biogeochemical cycling (Burden et al., 2013), topographic complexity (Lawrence
84 et al., 2018) and HWL attenuation (Kiesel et al., 2019). Burden et al., (2013) and Garbutt and
85 Wolters (2008) suggested that the difference between natural and restored saltmarshes may
86 be a function of time, as it may take up to 100 years for a restored marsh to reach
87 equivalence. The discrepancies between natural and restored saltmarshes reveal that
88 substantial knowledge gaps still exist when it comes to recreating both the habitat and its
89 ecosystem functioning.
90 These knowledge gaps may originate from the complex nature of coastal evolution and its
91 interaction with the original scheme design. Erosion and sedimentation give rise to changes
92 in site morphology (e.g. breach evolution: Friess et al., 2014; Vandenbruwaene et al., 2015),

93 which in turn provides new environmental conditions to the process regime. Such
94 interrelationships are further complicated by changing baselines, such as longer-term
95 changes in external forcing from modified storm climates, coastal sediment availability and,
96 in the future, accelerated sea level rise (van Goor et al., 2003). This significantly complicates
97 the numerical modelling of the MR site's morphodynamic evolution before and after
98 breaching (Friess et al., 2014; Symonds et al., 2008).
99 Esteves (2014) argued that it is important to assess whether the selected breach design allows
100 for the complete tidal drainage of a MR site of a particular size, especially during high water
101 events. Similarly, Stark et al. (2016) found that storage area limitations for floodwater might
102 cause water blockage against dikes, which in turn may result in HWL amplification. This may
103 explain why the close coupling between inundation depth and HWL attenuation within
104 saltmarshes (Stark et al., 2015) may be altered within MR sites (Kiesel et al., 2019). In order
105 to establish effective design guidelines for MR sites at the open coast, and to foster a stronger
106 public support and confidence for this management practice, detailed knowledge on the
107 effects of scheme design (size and breach design) on within-site HWL attenuation needs to
108 be obtained.
109 For example, the size of MR and its specific breach design determines the volume of water
110 between mean low and mean high water (Friess et al., 2014), which drives site internal
111 inundation depths. The latter has been shown to be correlated with HWL attenuation (Stark
112 et al., 2016; Stark et al., 2015). It is therefore crucial to revive the debate on whether to
113 perform bank removal or breach restoration, which arguably still constitutes "one of the
114 unresolved problems facing the UK intertidal restoration program" (Pethick, 2002 434).

This problem has been illustrated in the MR site of Freiston Shore, where HWL amplifications were observed during a field survey (Kiesel et al., 2019). Thus, the coastal protection function for which Freiston was designed is not fully realised. In this study, we present the results of a 2-D hydrodynamic model, calibrated and validated against field measurements of the highest spring tides of the year between August and October 2017, taken within, and seaward of, the Freiston Shore MR site (Kiesel et al., 2019). We investigate six potential adaptations to Freiston Shore (termed hereafter as scheme design scenarios) in order to explore the potential of improving the HWL attenuation of the MR site. We structure the scenarios in three groups; 1) two scenarios with three breaches and varying MR areas, 2) three single breach scenarios of different width and 3) one bank removal scenario. We furthermore discuss the implications of potential morphodynamic adjustments within each of these adaptations, by providing an analysis of bed shear stress for each scenario. Bed shear stress constitutes a useful parameter for this purpose, as it provides insights into depositional and erosional dynamics of intertidal areas (Callaghan et al., 2010; Li et al., 2019; Widdows et al., 2008).

## 2. Material and Methods

### *2.1 Study Area*

The Freiston Shore MR site is located on the shores of The Wash embayment in Lincolnshire, eastern UK (Fig. 1).

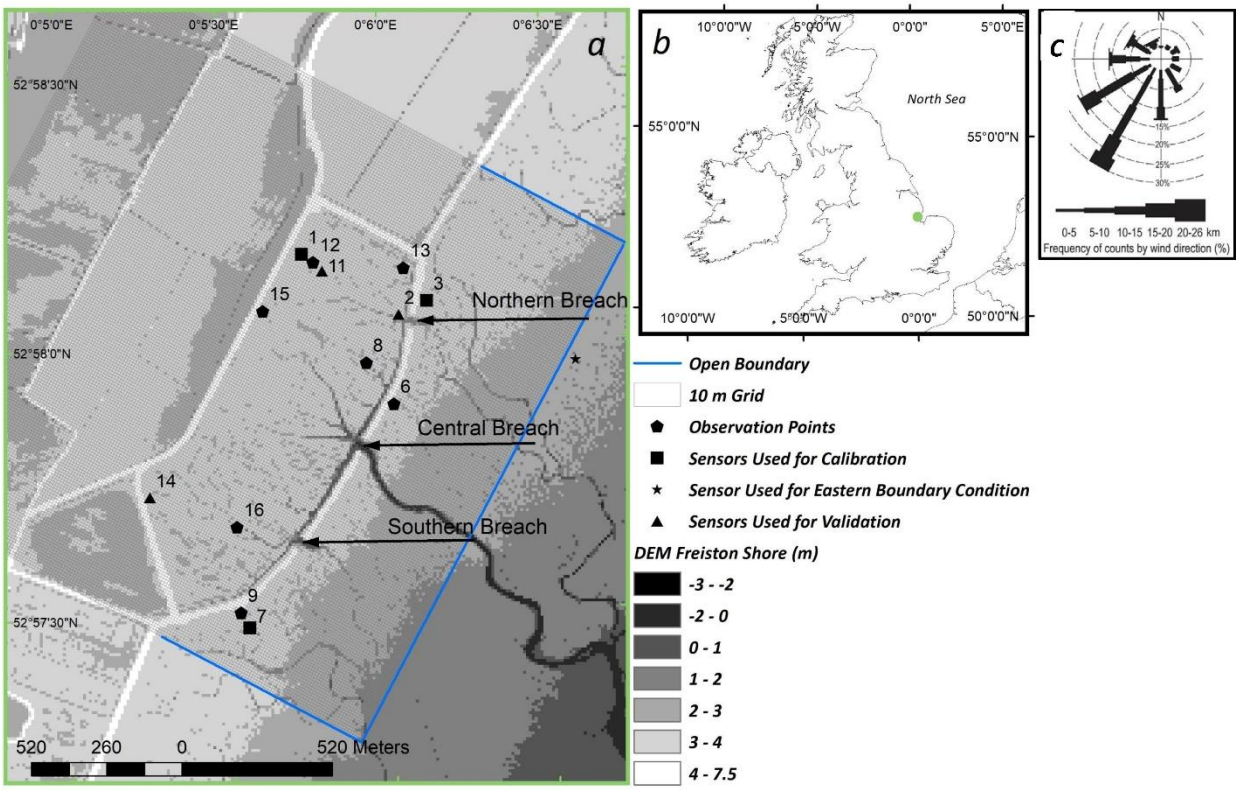


*Figure 1: Location of the Freiston Shore MR site (green dot) in eastern England, UK (b). Panel a) shows the model domain and observation points used for model calibration, validation and for the assessment of HWL attenuation rates. The underlying 10 x 10 m digital elevation model was derived from a 2016 Light Detection and Ranging (LiDAR) survey and was provided by the UK Environment Agency. Panel c was taken from Kiesel et al. (2019) and shows the wind conditions during the measurement period at Holbeach weather station, 18 km to the south of the study site. UK Met Office provided the wind data.*

135

136 The Wash comprises an area of about 600 km² (ca. 25 km long from southwest to northeast,
137 approximately 18 km wide from northwest to southeast at its seaward margin, and about 27
138 km wide towards its southern margin) with an average depth of < 10 m and maximum depths
139 between 40 – 50 m. The coastline of The Wash has a total length of 110 km, which is fringed
140 by intertidal environments including saltmarshes, mud- and sandflats (Brew and Williams,
141 2002). Southwesterly winds are dominant in The Wash, which was also the case during the
142 measurement period (Fig. 1c). The Wash has a semi-diurnal, macro tidal regime. Mean neap
143 and spring tidal range is 3.5 m and 6.5 m respectively, with flood-dominated tidal asymmetry

144 at the coastal margins (Friess et al., 2012; Ke et al., 1996; Pye, 1995). Between May 1999 and
145 May 2000, wave rider buoy measurements at the entrance to the Wash recorded maximum
146 wave heights of 2.81 m and mean significant wave heights of 0.61 m. These conditions make
147 The Wash a relatively low-energy embayment, which acts as a sink of marine sediments
148 (Spencer et al., 2012), while fluvial sediment inputs are minimal (Ke et al., 1996). Sediment
149 transport is consequently dominated by tidal currents, although waves have significantly
150 shaped the morphology of The Wash´s margins (Pye, 1995).
151 Hill and Randerson (1987) stated that 10 % of the UK´s saltmarsh area was located in The
152 Wash at the time of their investigation, comprising a total of 4,199 ha. In the 1990´s, 75 % of
153 The Wash´s coastline was fronted by saltmarsh (Pye, 1995). The shallow intertidal flats of The
154 Wash have been subject to extensive land reclamations since the medieval period up until
155 the 1980s (Doody, 1987). Between 1970 and 1980 alone, 800 ha of natural saltmarsh area
156 was reclaimed for agricultural use (Baily and Pearson, 2007). The latest seawall in this
157 sequence was created at Freiston Shore in 1982 (Symonds and Collins, 2005; Symonds and
158 Collins, 2007a; Symonds and Collins, 2007b), resulting in the retreat of the seaward edge of
159 the fronting natural saltmarsh at rates of 15 m $a^{-1}$ (Brew and Williams, 2002). Because of the
160 reduced buffer zone, which left the seawall at high risk of breaching, the 1996 regional
161 Shoreline Management Plan recommended realignment of this part of The Wash (Friess et
162 al., 2008). This was finally realized in August 2002 by setting the coastal defence back to an
163 earlier position, allowing for the restoration of formerly reclaimed saltmarshes over an area
164 of 66 ha.

Besides the reinforcement of the landward seawall (0.4 – 0.5 km inland), the realignment was undertaken by excavating three breaches (each of ca. 50 m width) in the seaward embankment. These breaches connected 1,200 m of artificially created tidal creeks within the site with those of the adjacent natural marsh in front of the site (Friess et al., 2014; Symonds and Collins, 2005; Symonds and Collins, 2007a). It was anticipated that the Freiston Shore MR site would fully inundate 150 times per year, which would allow for the development of mid to upper marsh communities, located above mean high water level (Nottage and Robertson, 2005).

Monitoring of the MR was organized by the UK Government´s Department for Environment, Food and Rural Affairs (DEFRA), the Environment Agency (EA) and the UK´s Natural Environmental Research Council´s Centre for Ecology and Hydrology (NERC CEH) and included the Cambridge Coastal Research Unit (University of Cambridge) and Birkbeck, University of London. The monitoring involved an assessment on vegetation development, accretion rates and invertebrates (Brown et al., 2007; Friess et al., 2012). The results confirmed the suitability of the site for rapid vegetation development; by 2007, the mean total halophytic vegetation cover within the MR was estimated at 89 %. In late summer 2017, the most abundant species present were *Salicornia europaea*, *Suaeda maritima*, *Puccinellia maritima*, *Atriplex portulacoides* and *Aster tripolium* (Kiesel et al., 2019).

The established vegetation and the additional shallow water area provided by the restored saltmarsh were expected to provide “within-marsh attenuation” of waves and water levels (Smolders et al., 2015), allowing the landward seawall to be of a lower design specification and thus, cheaper to build and maintain (Dixon et al., 1998; Pethick, 2002).

187 In 2005, elevations at 41 surface elevation table locations within the MR varied between 2.76
188 m and 3.26 m ODN (Ordnance Datum Newlyn, where 0.0 m ODN approximates to mean sea
189 level). In the first five years after breaching (2002 – 2007) most monitoring sites built up
190 between 6 – 73 mm sediment, while some sites nearest to the central breach showed an
191 exceptionally high total sedimentation of up to 215 mm (Brown et al., 2007). The latter
192 sedimentation rates were most likely a result of high localized sediment input from breach
193 and channel enlargement (Friess et al., 2014; Symonds and Collins, 2007a) and the
194 comparatively low surfaces as a result of the 1982 embanking (Spencer et al., 2012). After
195 MR implementation, average internal elevations used to be lower (generally <0.3 m)
196 compared to the adjacent natural marsh (Friess et al., 2012). Sediment accretion inside the
197 scheme has presumably sustained beyond the scope of the monitoring report, as in 2016 the
198 mean elevation inside the MR (3.04 ± 0.42 m ODN) was higher compared to the external
199 natural marsh (2.88 ± 0.5 m ODN) (Kiesel et al., 2019).
200
201 *2.2 Model Setup*
202 Flow of water over the model domain was simulated using the Delft3D-FLOW (version
203 4.00.02) model (Delft Hydraulics, 2003). Delft3D-FLOW allows for the computation of flow
204 and sediment transport over a multi-dimensional (2D (depth averaged) and 3D) finite,
205 rectilinear or curvilinear difference grid (Delft Hydraulics, 2003; Temmerman et al., 2012). A
206 2D depth averaged computation was used to solve the unsteady shallow-water equations.
207 Two-dimensional (depth-averaged) tide-induced flow was simulated on a Cartesian grid using
208 the horizontal momentum equations, the continuity equation and 2D turbulence, which was

209 modelled based on a constant horizontal eddy viscosity coefficient (1 $m^2 s^{-1}$). The modelled
210 period extended over the highest spring tides of the year 2017, from the 20th of September
211 to the 16th of October, applied at a time-step of six seconds. The model domain covered an
212 area of 1.97 km width and 1.95 km length, extending from the pioneer zone of the natural
213 saltmarsh in front of the MR over the MR itself in landward direction, up to the neighbouring
214 agricultural fields (Fig. 1).
215 A 2 x 2 m LiDAR (Light Detection and Ranging) based DEM from 2016 (provided by the UK
216 Environment Agency) was used to implement the bathymetry and topography of the Freiston
217 Shore coastal zone. This dataset was resampled to a 10 m x 10 m and 5 m x 5 m resolution
218 grid (the latter only for calibration purposes; see section 2.3) in order to reduce
219 computational costs. A bilinear resampling technique was applied in both cases, which uses
220 the average of the four nearest cells weighted by distance to define the new value of a cell.
221 The bathymetry in the model domain is consequently not reflecting the highest surface levels,
222 but includes sub grid scale features such as smaller tidal creeks, which are important for the
223 undisturbed flow in the study site.
224 Key surface covers were differentiated for the application of bottom roughness coefficients.
225 A supervised image classification (from Kiesel et al., 2019; overall accuracy of 93 %) was used
226 to distinguish between four different surface cover classes (saltmarsh, water, mud and
227 pasture). This classification was based on vertical aerial photography of 20 x 20 cm resolution,
228 which was taken on 6 May 2016 during low tide for the UK Environment Agency. The results
229 of the classification were validated by comparing twelve classified pixels to ground reference
230 measurements (Kiesel et al., 2019).

231 The model was forced with hourly meteorological data on wind speed and direction
232 measured at Holbeach weather station, 18 km south of the study site (Kiesel et al. 2019). It
233 was assumed that the wind pattern was homogeneously distributed over the comparatively
234 small model domain.
235 The hydrodynamic forcing of the eastern open boundary was defined in 10-minute intervals,
236 using water levels measured in 2017 in the direct vicinity (Fig. 1, Kiesel et al. 2019). The two
237 neighbouring open boundaries, situated perpendicular to the eastern boundary, were not
238 forced, but allowed to exchange water with the water body outside the model domain.
239
240 *2.3 Model Calibration and Validation*
241 The model was calibrated with tidal water depths measured at three locations (Loc 1, Loc 3,
242 Loc 7) within and outside the Freiston Shore MR site (Fig. 1). In order to test the model
243 performance, we compared between modelled and measured water depth. The deviation
244 between both was assessed by calculating root mean square errors (RMSE), mean errors (ME)
245 and mean absolute errors (MAE) for the entire inundated period, as well as RMSEs ($RMSE_{HWL}$)
246 and MAEs ($MAE_{HWL}$) of HWLs.
247 During calibration, the model was analysed for variations in the following model setups and
248 parameters: mesh size (10 m vs 5 m), 2D, 3D (the latter exhibiting both five and two layers),
249 Manning´s *n* roughness coefficients for saltmarsh surfaces (0.035 – 0.09), wind (including 2
250 sets of wind drag coefficients and one model run without wind included), reflection
251 parameter alpha (250 – 1000), boundary conditions (only eastern boundary forced vs. all
252 three boundaries forced) and time step (0.01 – 0.1 minutes). Best results were obtained by

253 retaining Delft3D-FLOW's default wind drag coefficients), a grid size of 10 x 10 m, a reflection
254 parameter (*alpha*) of 500, 2D model grid, forcing only the eastern open boundary and by
255 applying a time step of six seconds.
256 The influence of wind on the modelled water levels is calculated in Delft3D-FLOW through
257 the relationship between drag force and wind speed described by three break point drag and
258 wind speed conditions. The influence of these coefficients was calibrated by running the
259 model with a) no wind drag, b) default Delft3D-FLOW wind drag coefficients (breakpoint A
260 coefficient = 0.00063 at windspeed 0 m $s^{-1}$; B coefficient = 0.00723 and C = 0.00723, both at
261 windspeeds of 100 m $s^{-1}$), and c) varying drag coefficients and breakpoint windspeeds for
262 breakpoints A (0.0015 at 0 m $s^{-1}$) and B (0.005 at 40 m $s^{-1}$) (Bastidas et al., 2016; Delft
263 Hydraulics, 2003).
264 The effects of a range of values for Manning´s *n* coefficient for saltmarshes (0.035, 0.06, 0.07,
265 0.08 and 0.09) on modelled water depths were tested against the field measurements. All
266 coefficients (besides 0.09 and 0.06) were taken from the literature (Lawrence et al., 2004;
267 Stark et al., 2016; Stark et al., 2017; Temmerman et al., 2012; Wamsley et al., 2010).
268 Generally, the Freiston Shore model was not sensitive towards varying values of Manning´s *n*
269 coefficient. The range of mean $MAE_{HWL}$ for the calibration points varied between 0.047 m
270 ($MAE_{HWL}$ Loc 1 = 0.03, Loc 3 = 0.03 and Loc 7 = 0.08) for a Manning´s *n* value of 0.06 and 0.08
271 ($MAE_{HWL}$ Loc 1 = 0.03, Loc 3 = 0.03 and Loc 7 = 0.08) and 0.057 m for a Manning's *n* coefficient
272 of 0.09 ($MAE_{HWL}$ Loc 1 = 0.07, Loc 3 = 0.03 and Loc 7 = 0.07). Consequently, the Manning´s *n*
273 values of 0.06 and 0.08 gave the best fit to the observation data. A Manning´s *n* coefficient of
274 0.08 was selected for our model runs as this value has has been used widely in similar studies

for saltmarsh areas and proven to be suitable for approximating the roughness of saltmarsh surfaces (Loder et al., 2009; Stark et al., 2016; Temmerman et al., 2012). To account for the bottom roughness of other surface cover classes present in the model domain, Manning's *n* coefficients for additional types of surface covers were assigned as follows: tidal flat (0.03), open water (0.02) and pasture (0.06). These values have been shown to be suitable for representing the drag forces of rough surfaces in a range of hydrodynamic model applications (Garzon and Ferreira, 2016; Hossain et al; Lawrence et al., 2004; Liu et al., 2013; Smolders et al., 2015; Stark et al., 2016; Temmerman et al., 2012; Wamsley et al., 2010; Wamsley et al., 2009).

Validation was performed by comparing modelled and measured water depths at three additional locations (Loc 2, Loc 11 and Loc 14) (Fig. 1, Tab. 1). Model validation (based on $MAE_{HWL}$) confirmed that water depths were well represented by the model across the site. The model outputs showed a phase shift of typically 10 minutes, and a maximum of 20 minutes; a constant correction of 10 minutes was therefore applied.

*Table 1: Results of model validation at three locations. Error measurements represent the difference between modelled and measured water depths.*

| | RMSE (m) | ME (m) | MAE (m) | $RMSE_{HWL}$ (m) | $MAE_{HWL}$ (m) | Mean $MAE_{HWL}$ (m) |
|---|---|---|---|---|---|---|
| loc 2 | 0.060 | -0.030 | 0.050 | 0.060 | 0.040 | |
| loc 11 | 0.050 | 0.0200 | 0.030 | 0.030 | 0.030 | 0.030 |
| loc 14 | 0.060 | 0.030 | 0.030 | 0.020 | 0.020 | |

We used bed shear stress as an indicator for expected morphological adjustments, which are triggered by changes in scheme design and used the Status Quo to assess the validity of this approach. We looked at the difference between two LiDAR derived digital elevation models of Freiston Shore from the years 2002 (the year of the original breach) and 2016, in order to assess areas within Freiston, which have accreted or were eroded in the respective period. This figure shows that, in accordance with the spatial distribution of bed shear stress, morphological change has mostly focussed around the breaches, within, and next to, the artificial tidal creeks (supplementary material, Fig. S1).

*2.4 Scheme Design Scenarios*

In order to investigate whether changing the design of the Freiston Shore MR site would affect HWL attenuations, the scheme design was artificially changed by manipulating both the dike topography and the breach bathymetry in the model grid.

For this analysis a baseline scenario (status quo) was modelled, which represents the original implemented scheme. Additionally, six MR site modifications were applied, based on the most commonly used MR designs for the purpose of coastal protection in the UK: entire bank removal (Scenario 1), single breach design (Scenario 2) and schemes with more than two breaches (Scenario 3) (Fig. 2). The scenario site design characteristics are displayed in Table 2. Multiple variations in width of the central breach in the single breach designs (Scenarios 2.1, 2.2, 2.3) were tested, ranging from 30 m to 99 m. The latter breach width was implemented to account for any potential breach widening consequent upon changes in site hydrodynamics (Friess et al., 2014; Symonds and Collins, 2007a). Additionally, two variations

316 in MR area for schemes with two or more breaches were tested (Scenario 3.1 and 3.2) to
317 study the influence of site size on HWL attenuation (Tab. 2). For these scenarios, the storage
318 area of the Freiston Shore MR site was increased by 118 % and 73 % for Scenario 3.1 and 3.2,
319 respectively (Tab. 2, Fig. 2).

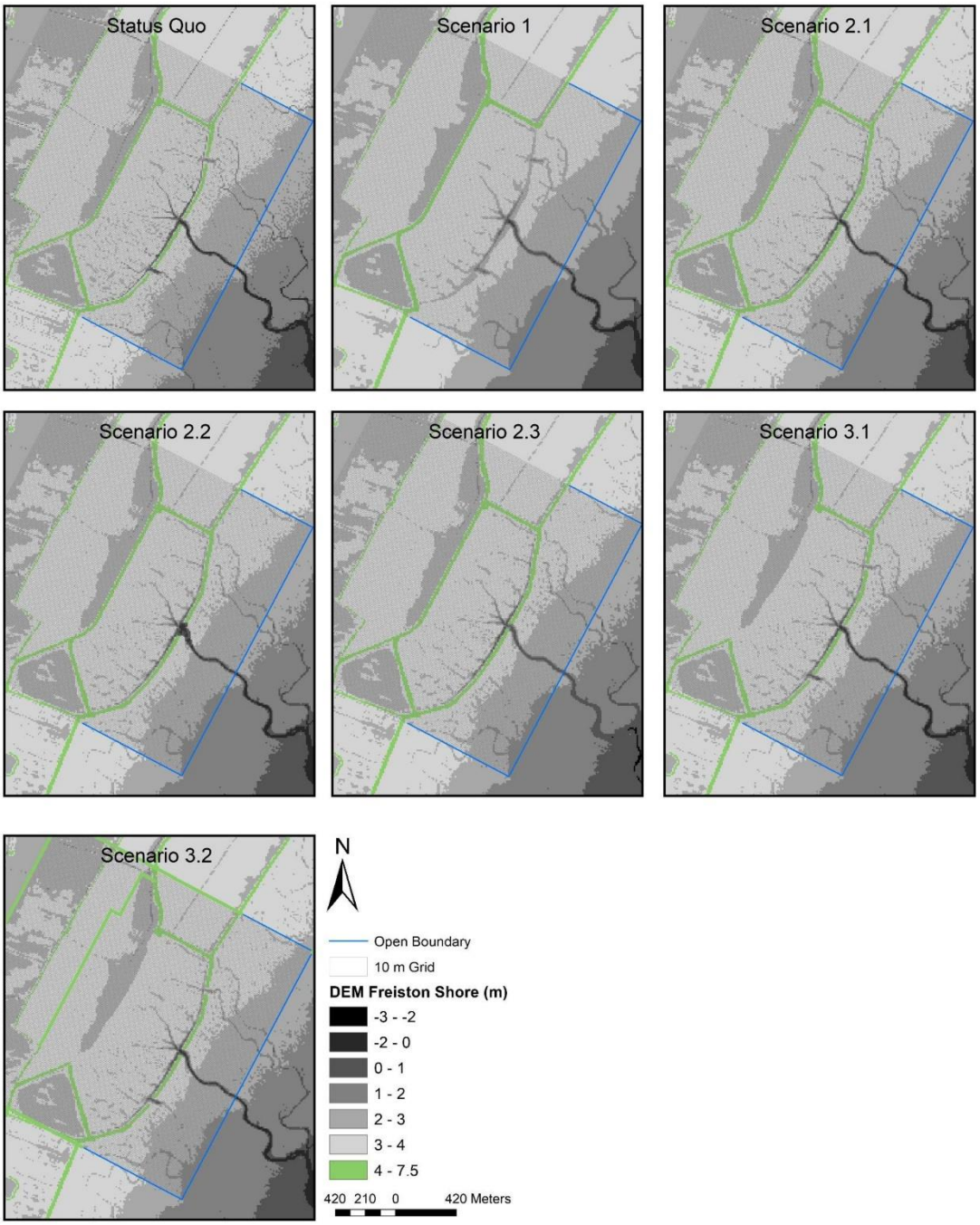


*Figure 2: Scheme design scenarios at the Freiston Shore MR site. The Status Quo constitutes the baseline scenario to which other models were compared. Scenario 1 represents a scheme design where the entire seawall has been removed. Scenario 2.1 depicts an alternative option with only one breach, while Scenario 2.2 constitutes a single breach scenario with an enlarged centre breach, accounting for expected morphologic adjustments, resulting from the closed northern- and southernmost breaches. In Scenario 2.3, the centre breach is decreased in size, in order to test the effects of a decreased tidal prism. In Scenario 3.1, the MR is significantly increased in size by removing the landward seawall to the back of the site. Scenario 3.2 is similar to Scenario 3.1, but characterised by a slightly smaller area. See Table 2 for further details.*

320

*Table 2: Number of breaches, total breach width and area for every MR scheme design scenario including the Status Quo.*

| | Status Quo | Scenario 1 | Scenario 2.1 | Scenario 2.2 | Scenario 2.3 | Scenario 3.1 | Scenario 3.2 |
|---|---|---|---|---|---|---|---|
| number of breaches | 3 | 1 | 1 | 1 | 1 | 3 | 3 |
| total breach width (m) | 127 | 1475 | 45 | 99 | 30 | 127 | 127 |
| MR area ($m^2$) | 650067 | 650067 | 650067 | 650067 | 650067 | 1416350 | 1124400 |

### *2.5 Calculation of HWL Attenuation Rates, Tidal Prism and Bed Shear Stress*

HWL attenuation rates (cm $km^{-1}$) were calculated from the vertical difference in water level (elevation based on bathymetry (see Tab. 3) + water depth) between two observation points (termed hereafter as transect) and the measured horizontal distance (m) between the two sensors. The following transects were assessed: Loc 13 – 1, Loc 3 – 1, Loc 2 – 1, Loc 11 – 1, Loc 8 – 15, Loc 6 – 15, Loc 16 – 14, and Loc 9 – 14 (Fig. 1). In order to assess the coastal protection function of the Freiston Shore MR site and the tested scenarios, we calculated HWL attenuation over transects, which range from seaward of the breached seawall to the reinforced landward seawall (Loc 3 – 1, Loc 6 – 15 and Loc 9 – 14). We additionally measured five transects from inside the MR to the landward seawall (Loc 13 – 1, Loc 2 – 1, Loc 11 – 1, Loc 8 – 15 and Loc 16 – 14). Positive rates refer to HWL attenuation, while negative values correspond to an amplification of HWLs along the respective transect (Kiesel et al., 2019).

The tidal prism ($m^3$) for each scenario was assessed by calculating the volume of water between average high and low water level within the MR during the measurement period. We used mean low water level and not just the marsh´s surface elevation to calculate the

tidal prism, because tidal creeks and depressions inside the MR always retained some water, even during low tide.

Bed shear stress was extracted from the model results for each cell and each time step. Afterwards, we averaged bed shear stress for every grid cell by exclusively taking periods of inundation into account.

*Table 3: Name, location and elevation of observation points used to calculate HWL attenuation rates. Elevation was extracted from the model bathymetry and the coordinates are given in British National Grid coordinate system.*

| Sensor # | Latitude | Longitude | Elevation based on Model Bathymetry (m ODN) |
|---|---|---|---|
| Loc 1 | 540728 | 343438 | 3.48 |
| Loc 2 | 541059 | 343229 | 3.23 |
| Loc 3 | 541154 | 343281 | 3.4 |
| Loc 6 | 541044 | 342920 | 3.39 |
| Loc 7 | 540544 | 342144 | 3.13 |
| Loc 8 | 540949 | 343061 | 3.24 |
| Loc 9 | 540518 | 342202 | 3.54 |
| Loc 11 | 540799 | 343378 | 3.29 |
| Loc 12 | 540768 | 343405 | 3.32 |
| Loc 13 | 541076 | 343390 | 3.1 |
| Loc 14 | 540205 | 342594 | 3.32 |
| Loc 15 | 540590 | 343239 | 3.32 |
| Loc 16 | 540503 | 342494 | 3.04 |

### *2.6 Statistical Analyses*

Since the data was neither normally distributed (Shapiro Wilk p-value < 0.0005) nor homoscedastic (Bartlett p-value < 0.0005), the non-parametric One-Way Wilcoxon rank sum

354 test and a Mann Whitney U test were used for statistical analysis. The latter was used to test
355 the hypothesis ($H_0$) that HWL attenuation rates of every scenario were not significantly
356 different from the status quo. The One-Way Wilcoxon rank sum test was used to investigate
357 the hypothesis ($H_0$) that HWL attenuation rates were not significantly different from zero.
358
359
360 **3 Results**
361 *3.1 The Effects of MR Scheme Design on HWL Attenuation*
362 To determine the overall effect of the MR on mean HWL attenuation rates for every scenario,
363 we first averaged attenuation rates over all measured transects and all high water events.
364 Hereafter, positive rates refer to the attenuation of HWLs, while negative values show that
365 HWLs were amplified.
366
367
368
369
370
371
372

373

374

375 Our results reveal statistically significant effects of the Freiston Shore MR scheme design on
376 HWL attenuation rates. HWL attenuation rates in all scenarios were significantly different
377 from zero and, besides Scenario 1, all scenarios were statistically significantly different from
378 the status quo (Fig. 3, Tab. 4).

379

*Table 4: Mean HWL attenuation rates, tidal prism and area for every scheme scenario including Status Quo. Standard deviations as well as p-values for the respective statistical tests are shown.*

380

| | Status Quo | Scenario 1 | Scenario 2.1 | Scenario 2.2 | Scenario 2.3 | Scenario 3.1 | Scenario 3.2 |
|---|---|---|---|---|---|---|---|
| Mean attenuation (cm $km^{-1}$) | -1 | -1 | 4 | 2 | 6 | 16 | 11 |
| Standard Deviation (cm $km^{-1}$) | 3 | 1 | 7 | 5 | 8 | 11 | 12 |
| One-Way Wilcoxon rank sum test (p-values) | 0.002 | < 0.0005 | < 0.0005 | < 0.0005 | < 0.0005 | < 0.0005 | < 0.0005 |
| Mann Whitney U test (p-values) | / | 0.5 | < 0.0005 | < 0.0005 | < 0.0005 | < 0.0005 | < 0.0005 |
| Tidal prism ($m^3$) | 296891 | 307435 | 263762 | 270122 | 256034 | 498752 | 420997 |
| Area ($m^2$) | 650067 | 650067 | 650067 | 650067 | 650067 | 1416350 | 1124400 |

381

382

While the status quo and Scenario 1 produced average attenuation rates of -1cm $km^{-1}$, indicating amplification of HWLs, all other scenarios produced average HWL attenuation, even though their minimum values reveal occasional amplification of HWLs (Fig. 3). HWL attenuation rates were highest for those scenarios where the three breaches remained intact and the MR area was substantially increased (Scenarios 3.1 and 3.2). Scenario 3.1 exhibited the highest attenuation rates, with attenuation rates of up to 73 cm $km^{-1}$.

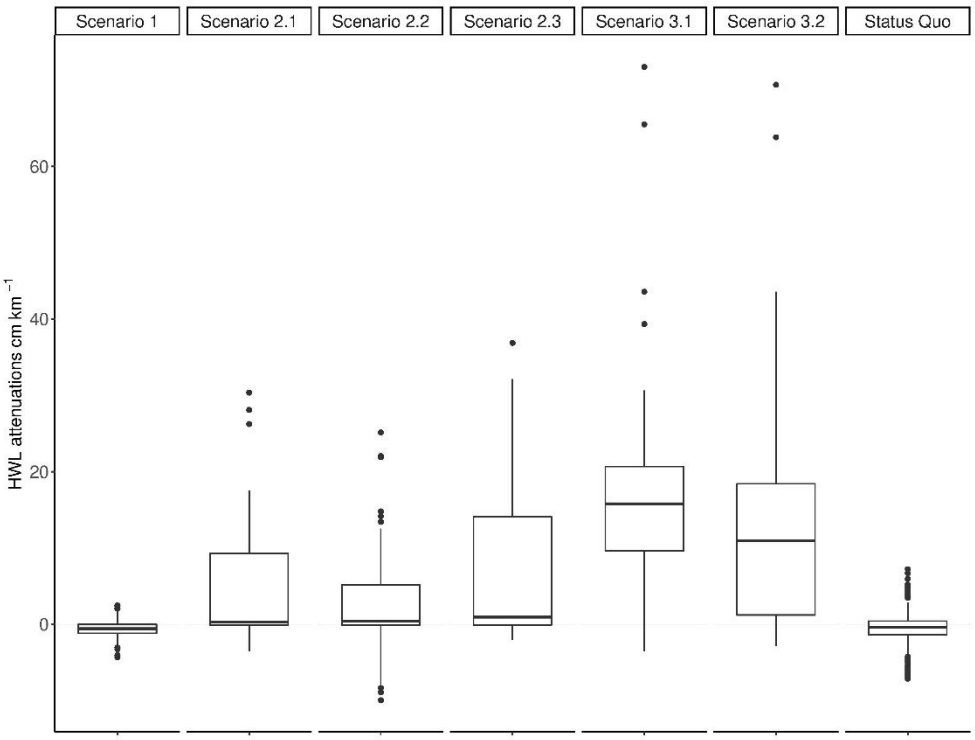


*Figure 3: HWL attenuation rates for all tested scheme design scenarios. Every boxplot represents the variation of HWL attenuation rates over all transects and all high water events of the respective scenario. The bottom and top ends of the box refer to the 25th and 75th percentile and the centreline constitutes the median. Both whiskers are calculated as the upper and lower boundary of the box + 1.5 * the interquartile range. Data points, which did not fall within this range, are plotted as outliers.*

390 HWL attenuation rates between individual transects shows no distinct spatial trends and
391 great variability across the MR in Scenario 1 and the status quo (Fig. 4). However, spatial
392 patterns can be observed for Scenarios 2 and 3. In Scenarios 2.1, 2.2 and 2.3 we found above
393 average attenuation rates for transects Loc 3 – 1, Loc 6 – 15 and Loc 9 – 14. In contrast to the
394 other transects, these were measured starting from in front of the old and breached dike.
395 This trend is also evident in Scenarios 3.1 and 3.2, but less distinct. In Scenario 3.1, lowest

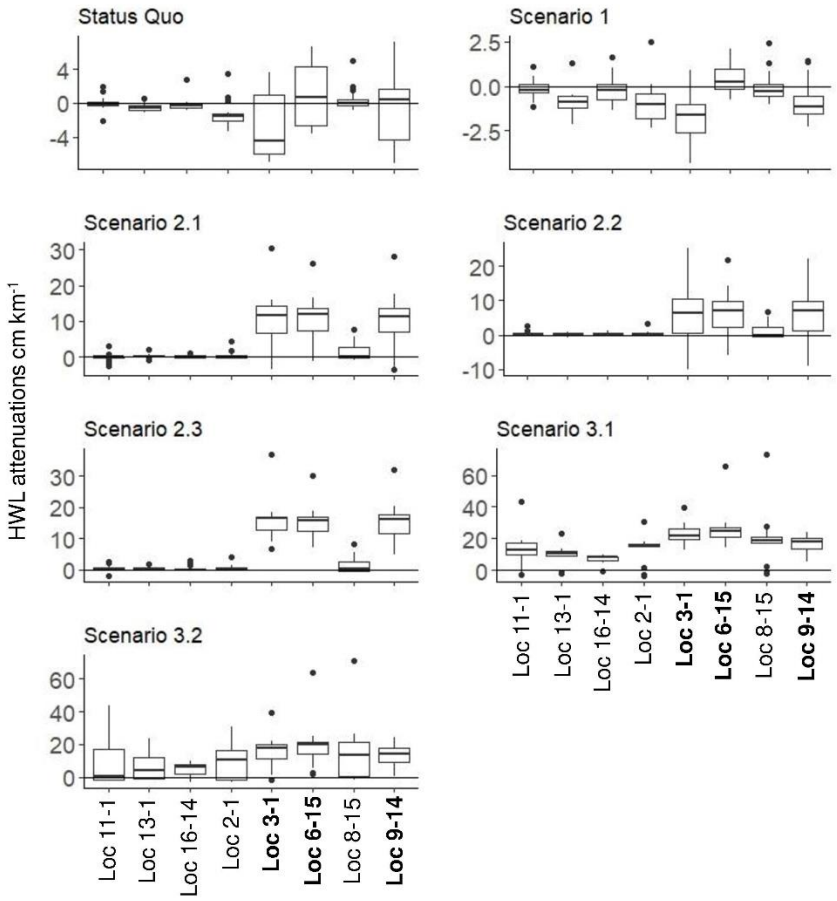


*Figure 4: HWL attenuation rates for every transect of each scenario. Every boxplot represents the variation of HWL attenuation rates over all high water events of the respective scenario. Note that the y-axes vary in scale in order to enhance the readability. Transect written in bold letters on the x-axes indicate those ranging from outside the breached seawall to the new, landward seawall. The bottom and top ends of the box refer to the 25$^{th}$ and 75$^{th}$ percentile and the centreline constitutes the median. Both whiskers are calculated as the upper and lower boundary of the box + 1.5 * the interquartile range. Data points, which did not fall within this range, are plotted as outliers.*

(yet still higher compared to all other scenarios) attenuation rates were assessed for transect Loc 16 – 14.

*3.2 Correlation of HWL Attenuation with Mean High Water Depth (MHWD)*

All scenarios, as well as the status quo, differ in terms of tidal prism (Tab. 4). The latter is determined by the respective area of the MR, as well as the breach design. Both determine the mean high water depth (MHWD) within the site, which is described by

$$MHWD = tp/A,$$

where *tp* refers to the site´s tidal prism ($m^3$) and *A* to MR area ($m^2$).. Our results indicate the dependency of HWL attenuation rates on MHWD, as a significantly negative correlation (p-value of polynomial model < 0.0005) was found across all scenarios (Fig. 5).

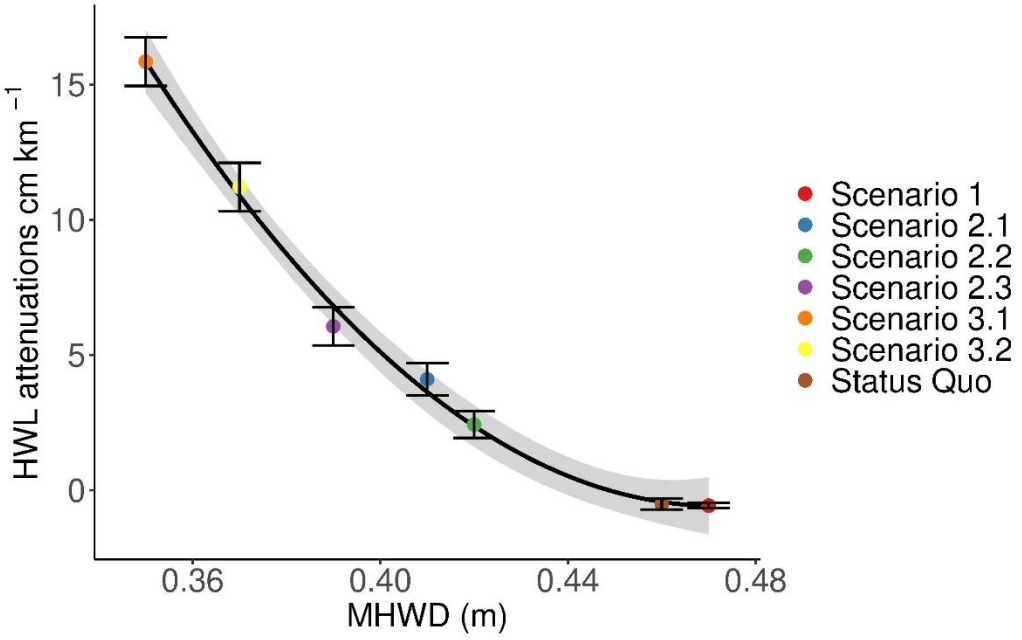


*Figure 5: The correlation between mean HWL attenuation of each scenario and MHWD. The error bars show the standard error of the mean and the shaded area around the polynomial model indicates the 95 % confidence interval. Formula: $y = 5.5 – 14 x + 4.3x^2$; $R^2 = 0.996$; adjusted $R^2 = 0.994$; $p < 0.0005$.*

Similarly, we found significant correlations (described by polynomial functions) between average HWL attenuation and mean high water depth of each individual high water event within each scenario (Fig. 6). The threshold, which divides between attenuation and amplification, is very different between scenarios. While for the status quo the threshold is approximately 0.4 m of mean high water depth, it increases by more than two-fold for scenarios 2.1, 2.2 and 3.2. For scenarios 2.3 and 3.1., the threshold water depth was not reached during the measurement period.

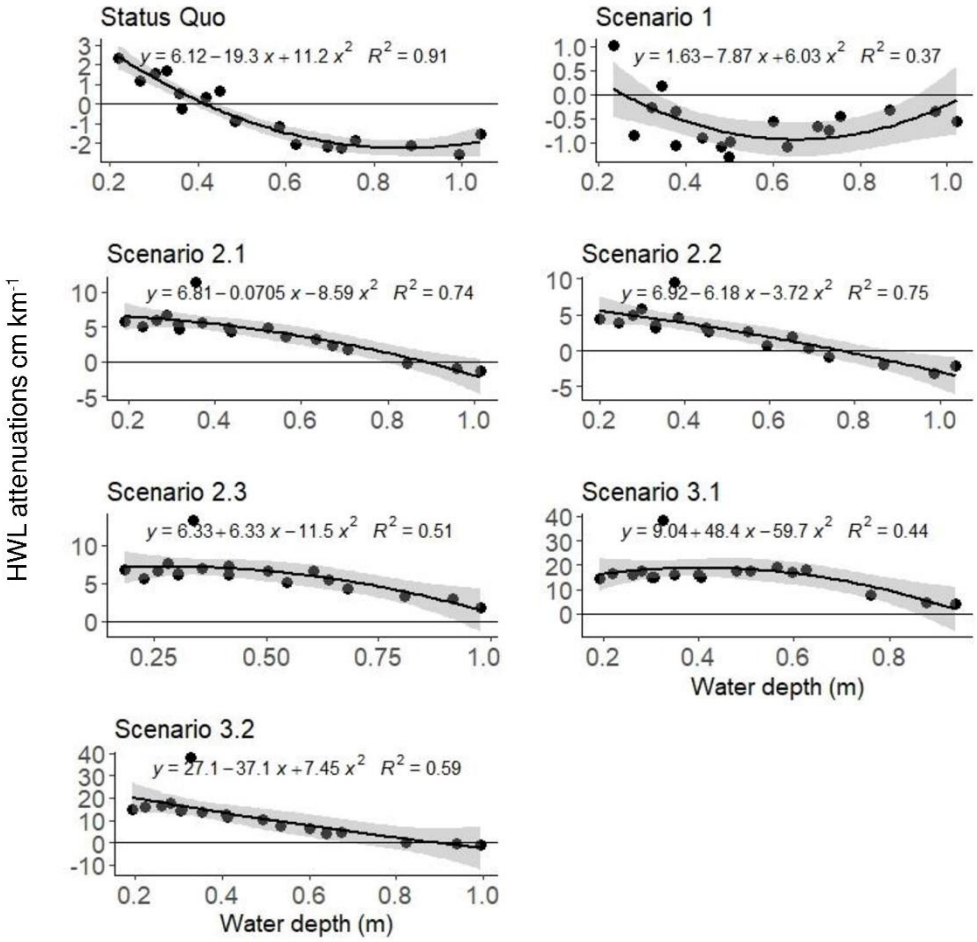


*Figure 6: Correlation between average HWL attenuation and mean high water depth. HWL attenuation has been averaged for every individual high water event during the simulated period by using all available transects. Mean high water depth has been calculated for every high water event and over all observation points within each MR scenario. The shaded area around the polynomial model represents the 95 % confidence interval.*

416

417

418

419

420

421 *3.3 Bed Shear Stress*

422 Our results show that areas of comparatively high bed shear stress are in all scenario families
423 mostly limited to the seaward edges of the MR site. Bed shear stress is generally highest
424 around the breaches, which is why it is extensively spread along the removed seawall in
425 Scenario 1 (Fig. 7).


*Figure 7: Bed shear stress within the three scenario families. Bed shear stress was averaged over the study period, excluding times when the site was not flooded.*

426 In Scenario 2.1, the highest values of bed shear stress are concentrated around the central
427 breach, whereas areas to the back of the site, including the north-eastern and south-western
428 parts, are characterised by comparatively low bed shear stress. In Scenario 3.1, high values
429 of bed shear stress also concentrate around the three breaches, but in comparison to
430 Scenarios 1 and 2.1, they are more scattered towards the northwest of the site, where the
431 landward seawall has been removed.

432

## 4 Discussion

### *4.1 Implications for MR Scheme Design*

Storage area and breach design of the Freiston Shore MR site have had a significant effect on the site´s HWL attenuation capacity. Furthermore, HWL attenuation can indeed be controlled by means of breach design. For example, when the storage area of the Freiston Shore MR site was kept constant (as in Scenario 1, 2, 2.2, 2.3 and the status quo), modelled HWL attenuation rates increased with decreasing tidal prism. In these scenarios, the tidal prism was controlled by changing the number and the widths of the breaches. However, our results show that effective coastal protection in terms of higher HWL attenuation rates (i.e. > 10 cm $km^{-1}$) can only be obtained if the MR area is of sufficient size. The maximum modelled HWL attenuation rates were observed for Scenarios 3.1 and 3.2 (up to 73 cm $km^{-1}$), which contained the largest storage areas and consequently exhibited the largest tidal prisms. Stark et al. (2015) measured comparable maximum HWL attenuation rates (up to 70 cm $km^{-1}$) over short transects in the extensive natural Saeftinghe marsh in the Western Scheldt estuary (Netherlands). We note, however, that a larger MR surface area provides also more space for wind waves to develop within the scheme, which may affect the development of vegetation, sedimentation patterns and ultimately, hydrodynamics (Nottage and Robertson, 2005).

Scenario 3.1 and 3.2 produced the highest attenuation rates because of their association with the lowest MHWD. This relationship helped explain most of the variation in mean HWL attenuations across scenarios, which was also observed for each scenario individually (Fig. 5, 6). However, previous studies have shown that also MR site orientation, meteorological

conditions, vegetation characteristics and local tidal regime are important drivers of HWL attenuation (Kiesel et al., 2019; Paquier et al., 2017; Resio and Westerink, 2008; Sheng et al., 2012; Stark et al., 2015; Wamsley et al., 2010; Wamsley et al., 2009). This hinders the extrapolation of HWL attenuation rates, measured at a given study site for a specific range of high water events and meteorological conditions, to other MR sites. The diverse driving forces of HWL attenuation help explaining why flood level reduction is highly variable between wetlands, specific wetland locations as well as individual high water events (Temmerman et al., 2012). This variability may be reflected in weaker correlations of HWL attenuation and the mean high water depth of each high water event within the scenarios (Fig. 6), when compared to the overall trend (Fig. 5).

We hypothesize that the close coupling between MHWD and HWL attenuation suggested by this study may vary depending on whether MR sites or natural marshes are considered. For example, this study suggests that scheme scenarios with MHWDs of > 0.4 m (Status Quo and Scenario 1) may already result in overall HWL amplification. This finding raises two major issues: i) problematically, HWL attenuation is particularly important when inundation depths are well above 0.4 m, for example during storm surge conditions; and ii) Stark et al. (2015), analysing field data, showed that for the extensive (natural) *Saeftinghe* marsh along the Western Scheldt estuary (Netherlands), HWL attenuation rates peaked during inundation depths ranging between 0.5 and 1 m. The latter provides reference that MR schemes (15 years of age) may not be as effective as natural marshes when it comes to the magnitude of HWL attenuation.

Consequently, future MR design needs to account for the altered correlation between MHWD and HWL attenuation within MR schemes and for the strong internal dynamics in attenuation rates. The former may enable the optimization of MR scheme designs for the purpose of "within-wetland" (Smolders et al., 2015) attenuation and thus, coastal protection. By measuring water depth as a function of MR area and local tidal prism, the usage of MHWD may help estimate the HWL attenuation potential of existing MR sites. This could enable the identification of sites with low or even negative HWL attenuation potential. For such sites, it could be possible to retro-fit an improved scheme design, by managing the site's tidal prism and / or the number, and width/s, of seawall breaches.

Breach design can be essential for coastal protection. Across most scenarios (all but Scenario 1), median and/or maximum HWL attenuation rates were highest for transects, which were measured from in front of the breached seawall (Fig. 4). For sites with a bank removal design, the approach to retro-fit an improved scheme design may, however, come too late.

At Freiston Shore, breach width and depth was, in the early stages of site evolution, dependent on the local tidal prism. This explains why after site implementation, breach channels increased in width by up to 950 % within only 2.5 month and shows that if breaches are designed with a cross sectional area insufficient to accommodate the tidal exchange, they are very likely to erode (Friess et al., 2014; Townend et al., 2016; Vandenbruwaene et al., 2015). This means that the breach design is restricted by local environmental circumstances. However, adverse effects could be prevented for sites, where the tidal prism is managed via regulated tidal exchange (21 of 74 UK MR sites) (ABPmer, 2019). In the UK, for example, regulated tidal exchange is usually not implemented for the purpose of coastal protection but

499 they may yet prove to be the most efficient in terms of HWL attenuation. However, regulated
500 tidal exchange may only offer a degree of control as the effects of meteorological conditions
501 acting on an enclosed body of water could still lead to adverse internal hydrodynamics and
502 HWL amplification (Kiesel et al., 2019).
503 Our findings emphasise the importance of breach design and regulated tidal exchange for MR
504 implementation. In contrast to bank removal (Scenario 1), breach design enables, even if only
505 to a limited extent, the regulation of the tidal prism and consequently, inundation depths,
506 which in turn determines the degree to which HWLs are attenuated within the MR site.
507 Furthermore, the remaining structure maintains a certain degree of protection for the
508 restored saltmarsh within the MR, increasing HWL attenuation rates (Fig. 4) and reducing the
509 erosional effects of storm waves and tidal currents and enhancing rapid sedimentation. This
510 may also be true for sites managed through regulated tidal exchange, as defences are
511 maintained and flow into the restoration site is controlled via culverts and sluices (Cox et al.,
512 2006; Esteves, 2014).
513
514 *4.2 Considerations on the Effects of Site Topography on Modelled HWL Attenuations*
515 In this paper, we evaluate the model results of each scenario based on the original
516 topography of the Freiston Shore MR site in 2016 (represented by a LiDAR derived digital
517 elevation model from 2016). We acknowledge that the morphology within each of the
518 scheme design scenarios would develop differently compared to the status quo, as tidal prism
519 and related hydrodynamics determine within-site sedimentation (Dale et al., 2017). This is
520 indicated by the spatial distribution of bed shear stress within the three scenario families.

Changes in marsh topography might be particularly expected for tidal channel geometry, as the latter is a function of the tidal prism (Friess et al., 2014). Marsh topography in terms of surface elevation and presence of tidal creeks affect HWL attenuation (Loder et al., 2009; Stark et al., 2016; Temmerman et al., 2012), which is why we expect HWL attenuation rates to change over time in each of the scenarios.

Stark et al. (2016) suggest that saltmarshes dominated by highly channelized flow provide less attenuation compared to marshes, which are dominated by sheet flow. This consideration suggests that the morphological evolution of MR sites could be critical to the coastal protection function in the long-term. It is therefore reasonable to assume that HWL attenuation rates presented for scenarios 3.1 and 3.2 are overestimated, as the newly created saltmarsh area to the back of the site would develop tidal creeks in order to drain and those creeks near the breaches would further expand in order to accommodate the increased tidal prism (Fig. 7). Unlike Scenarios 3.1 and 3.2, we assume that HWL attenuation rates are underestimated for scenario family 2. In Scenario 2.1, bed shear stress is low (compared to the Status Quo; Figure S1, Fig. 7) in the north-eastern and south-western parts. We would therefore assume the tidal creeks in these areas to fill up with sediments over time, resulting in increased sheet flow and ultimately, increased HWL attenuation rates for transects Loc 11 – 1, Loc 13 – 1, Loc 16 – 14, Loc 2 – 1, Loc 8 – 15. On the other hand, we found HWL attenuations to be exceptionally high for transects Loc 3 – 1, Loc 6 – 15 and Loc 9 – 14 (reaching from in front of the breached dike to the landward dike). Due to exceptionally high loads of bed shear stress within and next to the breaches of all scenarios (and particularly in the remaining central breach for scenario family 2), these transects will be most affected by

543 expected changes in channel morphology such as channel deepening and erosion and are
544 thus likely to be overestimated as well.
545
546 4.3 *Model Reproduces Water Depths But Not Variability in HWL Attenuations*
547 The model is well suited for the reproduction of measured water depths above the reference
548 plane (bathymetry) at several locations (Tab. 1). In addition, mean HWL attenuation for the
549 status-quo was found to be in the same order of magnitude between the model results (-1
550 cm $km^{-1}$) and the field survey (-3 cm $km^{-1}$) (Kiesel et al., 2019).
551 However, the exceptional variability of HWL attenuation rates measured inside the MR during
552 the original field survey (SD: 40 cm km-1) could not be reproduced by the model application
553 (SD: 3 cm km-1). The reasons for this discrepancy may involve the following four aspects: 1)
554 the transects over which HWL attenuations were measured differed between the original
555 field survey and this modelling study. 2) Uniform Manning n coefficients were used for all
556 vegetated surfaces, even though vegetation types assessed in the field revealed considerable
557 variations and 3), due to the use of averaged bathymetry and elevation data (10 x 10 m), the
558 model exhibited reduced topographic complexity. Furthermore, the reduced variability
559 within the model may be ascribed to 4) differences in elevation measurements at the
560 pressure sensor locations.
561 Accuracy of elevation measurements in the field (Leica Viva GS08 GNSS satellite survey (RTK))
562 are associated with an accuracy of up to 50 mm, but typically below 20 mm (Kiesel et al.,
563 2019). The bathymetry for the model presented in this study was derived from a 2 x 2 m LiDAR
564 digital terrain model measured in 2016 (provided by the UK Environment Agency) and

565 provided a vertical accuracy of ± 20 cm. In fact, this study found a systematic elevation
566 difference between the 10 x 10 m model bathymetry and the RTK measurements of, on
567 average, 0.47 m (Kiesel et al., 2019). Model bathymetry elevations were consistently higher
568 than the RTK measurements. It is known that due to the dense and low vegetation within
569 saltmarshes, LiDAR systems can fail to distinguish centimetre-scale variations between the
570 vegetation canopy (digital surface model) and the bare ground (digital terrain model)
571 (Hopkinson et al., 2004; Schmid et al., 2011). Schmid et al. (2011) ascribed this problem to
572 the poor penetration of the laser pulse through the marsh vegetation, which may result in
573 digital terrain models to be less accurate and significantly varying between different surface
574 types. This effect may be amplified by the high spatial heterogeneity of vegetation and
575 topographic features (Fernandez-Nunez et al., 2017).
576 This deviation can have a large effects on the calculation of HWL attenuation rates,
577 particularly over shorter marsh transects (Kiesel et al., 2019). The identified differences in
578 elevation measurements underline the difficulties that marsh vegetation and small scale
579 topographic variations pose on the derivation of elevation and bathymetry data. The
580 identified differences in elevation measurements highlight the importance of high-resolution
581 input data for the application of hydrodynamic models in coastal protection studies. This may
582 even be valid for areas with comparatively good data coverage, such as Freiston Shore.
583
584
585
586

## 5. Conclusion

MR schemes are generally designed based on well-established relationships between scheme design (e.g. surface area, breach dimensions/number and tidal prism) and hydrodynamic processes. The dependency of HWL attenuation on MR scheme design in this study has shown that these relationships do not necessarily predict HWL attenuation rates several years after breaching, particularly if site morphology and associated hydrodynamics change over time. We therefore stress the need for continued monitoring efforts in MR schemes.

We show that HWL attenuation is strongly dependent on within-site MHWD. The latter is not only a function of the well-established relationship between water depth, surface roughness and HWL attenuation but also incorporates the parameters of tidal prism and MR site area. Thus, once the available area for a MR site is known, the width(s) of the seawall breach(es) can be designed in order to accommodate a tidal prism, which result in the lowest possible MHWDs that allow for the attenuation of HWLs.

We suggest that breach design and regulated tidal exchange should be the preferred design options for MR sites that are implemented for the purpose of coastal protection. The reason is that both enable controlling the tidal prism (and consequently inundation depths) and because the breached seawall may additionally enhance HWL attenuation rates.

We also show that our hydrodynamic model application may not be able to capture the within-site dynamics of HWL attenuation. It is important to account for these dynamics, particularly when the protection standard of new seawalls at the landward margins of MR sites need to be determined. For now, the prediction of the effects of meteorological conditions and extreme events on the relationship between MHWD and HWL attenuation is

not fully understood. There is an urgent need for further field investigations of water level dynamics within MR sites, particularly under high water level, storm surge conditions.

**Acknowledgements**

The work presented in this paper is based on field data obtained during JK´s research stay at the Department of Geography´s Visiting Scholar programme of the University of Cambridge. JK particularly thanks B. Evans (Cambridge Coastal Research Unit) for technical and field assistance. Furthermore, JK thanks Pushpa Dissanayake for his helpful introduction to the Delft3D modelling environment and the Integrated School of Ocean Science as part of the Future Ocean Excellence Cluster (University of Kiel) for funding the original field campaign. The authors thank the UK Environment Agency, for the supply of vertical aerial photography, LiDAR data and for their fast and helpful responses to our requests regarding the data. Furthermore, the authors would like to thank Deltares Delft Hydraulics for providing the Delft3D-FLOW model. This is a contribution towards UKRI NERC BLUECoast project (NE/N015878/1).

## References

ABPmer, 2019. The Online Managed Realignment Guide. https://www.omreg.net/. Accessed 22 February 2019.

Baily, B., Pearson, A.W., 2007. Change detection mapping and analysis of salt marsh areas of central southern England from Hurst Castle Spit to Pagham Harbour. Journal of Coastal Research 236, 1549–1564. 10.2112/05-0597.1.

Bastidas, L.A., Knighton, J., Kline, S.W., 2016. Parameter sensitivity and uncertainty analysis for a storm surge and wave model. Nat. Hazards Earth Syst. Sci. 16 (10), 2195–2210. 10.5194/nhess-16-2195-2016.

Brew, D., Williams, A., 2002. Shoreline movement and shoreline management in The Wash, eastern England. Littoral conference 2002, the changing coast, Porto, Portugal, 313–320.

636 Brown, S.L., Pinder, A., Scott, L., Bass, J., Rispin, E., Brown, S., Garbutt, A., Thomson, A., Spencer, T.,
637 Möller, I., Brooks, S.M., 2007. Wash banks flood defence scheme Freiston environment monitoring
638 2002 - 2006. FD 1911/TR. Joint DEFRA/EA Flood and Coastal Erosion Risk Management R&D
639 Programme.
640 Burden, A., Garbutt, R.A., Evans, C.D., Jones, D.L., Cooper, D.M., 2013. Carbon sequestration and
641 biogeochemical cycling in a saltmarsh subject to coastal managed realignment. Estuarine, Coastal
642 and Shelf Science 120, 12–20. 10.1016/j.ecss.2013.01.014.
643 Callaghan, D.P., Bouma, T.J., Klaassen, P., van der Wal, D., Stive, M., Herman, P., 2010. Hydrodynamic
644 forcing on salt-marsh development: Distinguishing the relative importance of waves and tidal flows.
645 Estuarine, Coastal and Shelf Science 89 (1), 73–88. 10.1016/j.ecss.2010.05.013.
646 Cooper, J., McKenna, J., 2008. Working with Natural Processes: The Challenge for Coastal Protection
647 Strategies. Geogr. J. 174 (4), 315–331.
648 Cox, T., Maris, T., Vleeschauwer, P. de, Mulder, T. de, Soetaert, K., Meire, P., 2006. Flood control areas
649 as an opportunity to restore estuarine habitat. Ecological Engineering 28 (1), 55–63.
650 10.1016/j.ecoleng.2006.04.001.
651 Cross, M., 2017. Wallasea Island Wild Coast Project, UK: Circular economy in the built environment.
652 Proceedings of the Institution of Civil Engineers - Waste and Resource Management 170 (1), 3–14.
653 10.1680/jwarm.16.00006.
654 Dale, J., Burgess, H.M., Cundy, A.B., 2017. Sedimentation rhythms and hydrodynamics in two engineered
655 environments in an open coast managed realignment site. Marine Geology 383, 120–131.
656 10.1016/j.margeo.2016.12.001.
657 Day, J.W., Boesch, D.F., Clairain, E.J., Kemp, G.P., Laska, S.B., Mitsch, W.J., Orth, K., Mashriqui, H., Reed,
658 D.J., Shabman, L., Simenstad, C.A., Streever, B.J., Twilley, R.R., Watson, C.C., Wells, J.T., Whigham,
659 D.F., 2007. Restoration of the Mississippi Delta: lessons from Hurricanes Katrina and Rita. Science
660 (New York, N.Y.) 315 (5819), 1679–1684. 10.1126/science.1137030.
661 Delft Hydraulics, 2003. User Manual Delft3D-FLOW. WL. Delft Hydraulics, Delft, The Netherlands.
662 Dixon, A.M., Leggett, D., Weight, R.C., 1998. Habitat Creation Opportunities for Landward Coastal Re-
663 alignment: Essex Case Studies. Water Environ. 12 (2), 107–112.
664 Doody, J.P., 1987. Background to the conference, in: The Wash and its Environment. Nature
665 Conservancy Council, Peterborough, UK.
666 EPA, 2013. San Francisco Bay Delta Watershed. United States Environmental Protection agency.
667 http://www2.epa.gov/sfbay-delta. Accessed 8 November 2011.
668 Esteves, L.S., 2013. Is managed realignment a sustainable long-term coastal management approach?
669 Journal of Coastal Research 65, 933–938. 10.2112/SI65-158.1.
670 Esteves, L.S., 2014. Managed realignment: A viable long-term coastal management strategy? Springer,
671 New York.
672 Esteves, L.S., Thomas, K., 2014. Managed realignment in practice in the UK: results from two
673 independent surveys. In: Green, A.N., Cooper, J. (Eds.) proceedings 13th International Coastal
674 Symposium, Durban, South Africa, pp. 407–413.
675 Esteves, L.S., Williams, J.J., 2017. Managed realignment in Europe: a synthesis of methods, achievements
676 and challanges. In: Bilkovic, D.M., Mitchell, M.M., Toft, J.D., La Peyre, M.K. (Eds.) Living Shorelines:
677 The Science and Management of Nature-based Coastal Protection. CRC Press/Taylor & Francis
678 Group, pp. 157–180.

679 Fernandez-Nunez, M., Burningham, H., Ojeda Zujar, J., 2017. Improving accuracy of LiDAR-derived digital
680 terrain models for saltmarsh management. J Coast Conserv 21 (1), 209–222. 10.1007/s11852-016-
681 0492-2.
682 Friess, D., Möller, I., Spencer, T., 2008. Managed realignment and the re-establishment of saltmarsh
683 habitat, Freiston Shore, Lincolnshire, United Kingdom, in: The Role of Environmental Management
684 and Eco-Engineering in Disaster Risk Reduction and Climate Change Adaptation, pp. 65–78.
685 Friess, D.A., Möller, I., Spencer, T., Smith, G.M., Thomson, A.G., Hill, R.A., 2014. Coastal saltmarsh
686 managed realignment drives rapid breach inlet and external creek evolution, Freiston Shore (UK).
687 Geomorphology 208, 22–33. 10.1016/j.geomorph.2013.11.010.
688 Friess, D.A., Spencer, T., Smith, G.M., Möller, I., Brooks, S.M., Thomson, A.G., 2012. Remote sensing of
689 geomorphological and ecological change in response to saltmarsh managed realignment, The Wash,
690 UK. International Journal of Applied Earth Observation and Geoinformation 18, 57–68.
691 10.1016/j.jag.2012.01.016.
692 Garbutt, A., Wolters, M., 2008. The natural regeneration of salt marsh on formerly reclaimed land.
693 Applied Vegetation Science 11 (3), 335–344. 10.3170/2008-7-18451.
694 Garzon, J., Ferreira, C., 2016. Storm Surge Modeling in Large Estuaries: Sensitivity Analyses to
695 Parameters and Physical Processes in the Chesapeake Bay. JMSE 4 (3), 45. 10.3390/jmse4030045.
696 Hill, M., Randerson, P., 1987. Saltmarsh vegetation communities of The Wash and their recent
697 development, in: The Wash and its Environment. Nature Conservancy Council, Peterborough, UK.
698 Hopkinson, C., Lim, K., Chasmer, L.E., Treitz, P., Creed, I.F., Gynan, C., 2004. Wetland grass to plantation
699 forest - estimating vegetation height from the standard deviation of lidar frequency distributions. Int
700 Arch Photogramm Remote Sens Spat Inf Sci 36 (8/W2), 288–294.
701 Hossain, A., Yafei Jia, Xiabo Chao. Estimation of Manning's roughness coefficient distribution for
702 hydrodynamic model using remotely sensed land cover features, in: 2009 17th International
703 Conference on Geoinformatics, Fairfax, VA, pp. 1–4.
704 Ke, X., Evans, G., Collins, M.B., 1996. Hydrodynamics and sediment dynamics of The Wash embayment,
705 eastern England. Sedimentology 43, 157–174.
706 Kiesel, J., Schuerch, M., Möller, I., Spencer, T., Vafeidis, A., 2019. Attenuation of high water levels over
707 retored saltmarshes can be limited.: Insights from Freiston Shore, Lincolnshire, UK. Ecological
708 Engineering 136, 89–100.
709 Lawrence, D., Allen, J., Havelock, G.M., 2004. Salt Marsh Morphodynamics: an Investigation of Tidal
710 Flows and Marsh Channel Equilibrium. Journal of Coastal Research 20 (1), 301–316.
711 Lawrence, P.J., Smith, G.R., Sullivan, M.J., Mossman, H.L., 2018. Restored saltmarshes lack the
712 topographic diversity found in natural habitat. Ecological Engineering 115, 58–66.
713 10.1016/j.ecoleng.2018.02.007.
714 Ledoux, L., Cornell, S., O'Riordan, T., Harvey, R., Banyard, L., 2005. Towards sustainable flood and coastal
715 management: Identifying drivers of, and obstacles to, managed realignment. Land Use Policy 22 (2),
716 129–144. 10.1016/j.landusepol.2004.03.001.
717 Li, X., Leonardi, N., Plater, A.J., 2019. Wave-driven sediment resuspension and salt marsh frontal erosion
718 alter the export of sediments from macro-tidal estuaries. Geomorphology 325, 17–28.
719 10.1016/j.geomorph.2018.10.004.
720 Liu, H., Zhang, K., Li, Y., Xie, L., 2013. Numerical study of the sensitivity of mangroves in reducing storm
721 surge and flooding to hurricane characteristics in southern Florida. Continental Shelf Research 64,
722 51–65. 10.1016/j.csr.2013.05.015.

723 Loder, N.M., Irish, J.L., Cialone, M.A., Wamsley, T.V., 2009. Sensitivity of hurricane surge to
724 morphological parameters of coastal wetlands. Estuarine, Coastal and Shelf Science 84 (4), 625–636.
725 10.1016/j.ecss.2009.07.036.
726 Luisetti, T., Turner, R.K., Bateman, I.J., Morse-Jones, S., Adams, C., Fonseca, L., 2011. Coastal and marine
727 ecosystem services valuation for policy and management: Managed realignment case studies in
728 England. Ocean & Coastal Management 54 (3), 212–224. 10.1016/j.ocecoaman.2010.11.003.
729 Mazik, K., Musk, W., Dawes, O., Solyanko, K., Brown, S., Mander, L., Elliott, M., 2010. Managed
730 realignment as compensation for the loss of intertidal mudflat: A short term solution to a long term
731 problem? Estuarine, Coastal and Shelf Science 90 (1), 11–20. 10.1016/j.ecss.2010.07.009.
732 Möller, I., Kudella, M., Rupprecht, F., Spencer, T., Paul, M., van Wesenbeeck, B.K., Wolters, G., Jensen,
733 K., Bouma, T.J., Miranda-Lange, M., Schimmels, S., 2014. Wave attenuation over coastal salt marshes
734 under storm surge conditions. Nature Geosci 7 (10), 727–731. 10.1038/ngeo2251.
735 Möller, I., Spencer, T., 2002. Wave dissipation over macro-tidal saltmarshes: Effects of marsh edge
736 typology and vegetation change. Journal of Coastal Research (SI36), 506–521.
737 Mossman, H.L., Davy, A.J., Grant, A., Elphick, C., 2012. Does managed coastal realignment create
738 saltmarshes with 'equivalent biological characteristics' to natural reference sites? J Appl Ecol 49 (6),
739 1446–1456. 10.1111/j.1365-2664.2012.02198.x.
740 Nottage, A., Robertson, P., 2005. The saltmarsh creation handbook: A project manager's guide to the
741 creation of saltmarsh and intertidal mudflat / by Albert Nottage and Peter Robertson. Royal Society
742 for the Protection of Birds, Sandy.
743 Paquier, A.-E., Haddad, J., Lawler, S., Ferreira, C.M., 2017. Quantification of the Attenuation of Storm
744 Surge Components by a Coastal Wetland of the US Mid Atlantic. Estuaries and Coasts 40 (4), 930–
745 946. 10.1007/s12237-016-0190-1.
746 Pethick, J., 2002. Estuarine and Tidal Wetland Restoration in the United Kingdom: Policy Versus Practice.
747 Restoration Ecology 10 (3), 431–437.
748 Pye, K., 1995. Controls on Long-term Saltmarsh Accretion and Erosion in the Wash, Eastern England.
749 Journal of Coastal Research 11 (2), 337–356.
750 Resio, D.T., Westerink, J.J., 2008. Modeling the physics of storm surges. Physics Today 61 (9), 33–38.
751 10.1063/1.2982120.
752 Rupprecht, F., Möller, I., Paul, M., Kudella, M., Spencer, T., van Wesenbeeck, B.K., Wolters, G., Jensen,
753 K., Bouma, T.J., Miranda-Lange, M., Schimmels, S., 2017. Vegetation-wave interactions in salt
754 marshes under storm surge conditions. Ecological Engineering, 100, 301-315.
755 10.1016/j.ecoleng.2016.12.030.
756 Schernewski, G., Bartel, C., Kobarg, N., Karnauskaite, D., 2018a. Retrospective assessment of a managed
757 coastal realignment and lagoon restoration measure: The Geltinger Birk, Germany. J Coast Conserv
758 22 (1), 157–167. 10.1007/s11852-017-0496-6.
759 Schernewski, G., Schumacher, J., Weisner, E., Donges, L., 2018b. A combined coastal protection,
760 realignment and wetland restoration scheme in the southern Baltic: Planning process, public
761 information and participation. J Coast Conserv 22 (3), 533–547. 10.1007/s11852-017-0542-4.
762 Schmid, K.A., Hadley, B.C., Wijekoon, N., 2011. Vertical Accuracy and Use of Topographic LIDAR Data in
763 Coastal Marshes. Journal of Coastal Research 275, 116–132. 10.2112/JCOASTRES-D-10-00188.1.
764 Sheng, Y.P., Lapetina, A., Ma, G., 2012. The reduction of storm surge by vegetation canopies: Three-
765 dimensional simulations. Geophys. Res. Lett. 39 (20). 10.1029/2012GL053577.
766 Sigma Plan, 2011. https://www.sigmaplan.be/en/. Accessed 8 November 2019.

767 Smolders, S., Plancke, Y., Ides, S., Meire, P., Temmerman, S., 2015. Role of intertidal wetlands for tidal
768 and storm tide attenuation along a confined estuary: A model study. Nat. Hazards Earth Syst. Sci. 15
769 (7), 1659–1675. 10.5194/nhess-15-1659-2015.
770 Spencer, K.L., Harvey, G.L., 2012. Understanding system disturbance and ecosystem services in restored
771 saltmarshes: Integrating physical and biogeochemical processes. Estuarine, Coastal and Shelf Science
772 106, 23–32. 10.1016/j.ecss.2012.04.020.
773 Spencer, T., Brooks, S.M., Evans, B.R., Tempest, J.A., Möller, I., 2015. Southern North Sea storm surge
774 event of 5 December 2013: Water levels, waves and coastal impacts. Earth-Science Reviews 146,
775 120–145. 10.1016/j.earscirev.2015.04.002.
776 Spencer, T., Friess, D.A., Möller, I., Brown, S.L., Garbutt, R.A., French, J.R., 2012. Surface elevation
777 change in natural and re-created intertidal habitats, eastern England, UK, with particular reference
778 to Freiston Shore. Wetlands Ecol Manage 20 (1), 9–33. 10.1007/s11273-011-9238-y.
779 Stark, J., Plancke, Y., Ides, S., Meire, P., Temmerman, S., 2016. Coastal flood protection by a combined
780 nature-based and engineering approach: Modeling the effects of marsh geometry and surrounding
781 dikes. Estuarine, Coastal and Shelf Science 175, 34–45. 10.1016/j.ecss.2016.03.027.
782 Stark, J., Smolders, S., Meire, P., Temmerman, S., 2017. Impact of intertidal area characteristics on
783 estuarine tidal hydrodynamics: A modelling study for the Scheldt Estuary. Estuarine, Coastal and
784 Shelf Science 198, 138–155. 10.1016/j.ecss.2017.09.004.
785 Stark, J., van Oyen, T., Meire, P., Temmerman, S., 2015. Observations of tidal and storm surge
786 attenuation in a large tidal marsh. Limnol. Oceanogr. 60 (4), 1371–1381. 10.1002/lno.10104.
787 Symonds, A.M., Collins, M.B., 2005. Sediment dynamics associated with managed realignment; Freiston
788 Shore, The Wash, UK, in: Proceedings of the 29th International Conference, National Civil
789 Engineering Laboratory, Lisbon, Portugal. 19 – 24 September 2004, pp. 3173–3185.
790 Symonds, A.M., Collins, M.B., 2007a. The development of artificially created breaches in an
791 embankment as part of a managed realignment, Freiston Shore, UK. Journal of Coastal Research (SI
792 50), 130–134.
793 Symonds, A.M., Collins, M.B., 2007b. The establishment and degeneration of a temporary creek system
794 in response to managed coastal realignment: The Wash, UK. Earth Surf. Process. Landforms 32 (12),
795 1783–1796. 10.1002/esp.1495.
796 Symonds, A.M., Scott, C.R., Collins, M.B., 2008. Assessing the physical impacts of managed realignment
797 in an estuarine and coastal environment, in: Proceedings of the 31st International Conference,
798 Hamburg, Germany. 31 August – 5 September 2008, pp. 4508–4520.
799 Temmerman, S., Meire, P., Bouma, T.J., Herman, P.M.J., Ysebaert, T., Vriend, H.J. de, 2013. Ecosystem-
800 based coastal defence in the face of global change. Nature 504 (7478), 79–83. 10.1038/nature12859.
801 Temmerman, S., Vries, M.B. de, Bouma, T.J., 2012. Coastal marsh die-off and reduced attenuation of
802 coastal floods: A model analysis. Global and Planetary Change 92-93, 267–274.
803 10.1016/j.gloplacha.2012.06.001.
804 Townend, I., Wang, Z.B., Stive, M., Zhou, Z., 2016. Development and extension of an aggregated scale
805 model: Part 1 – Background to ASMITA. China Ocean Eng. (China Ocean Engineering) 30 (4), 483–
806 504. 10.1007/s13344-016-0030-x.
807 Turner, R.K., Burgess, D., Hadley, D., Coombes, E., Jackson, N., 2007. A cost–benefit appraisal of coastal
808 managed realignment policy. Global Environmental Change 17 (3-4), 397–407.
809 10.1016/j.gloenvcha.2007.05.006.

van Goor, M.A., Zitman, T.J., Wang, Z.B., Stive, M., 2003. Impact of sea-level rise on the morphological equilibrium state of tidal inlets. Marine Geology 202 (3-4), 211–227. 10.1016/S0025-3227(03)00262-7.

Vandenbruwaene, W., Schwarz, C., Bouma, T.J., Meire, P., Temmerman, S., 2015. Landscape-scale flow patterns over a vegetated tidal marsh and an unvegetated tidal flat: Implications for the landform properties of the intertidal floodplain. Geomorphology 231, 40–52. 10.1016/j.geomorph.2014.11.020.

Wamsley, T.V., Cialone, M.A., Smith, J.M., Atkinson, J.H., Rosati, J.D., 2010. The potential of wetlands in reducing storm surge. Ocean Engineering 37 (1), 59–68. 10.1016/j.oceaneng.2009.07.018.

Wamsley, T.V., Cialone, M.A., Smith, J.M., Ebersole, B.A., Grzegorzewski, A.S., 2009. Influence of landscape restoration and degradation on storm surge and waves in southern Louisiana. Nat Hazards 51 (1), 207–224. 10.1007/s11069-009-9378-z.

Widdows, J., Pope, N.D., Brinsley, M.D., 2008. Effect of Spartina anglica stems on near-bed hydrodynamics, sediment erodability and morphological changes on an intertidal mudflat. Mar. Ecol. Prog. Ser. 362, 45–57. 10.3354/meps07448.